International Journal of Biometeorology (2026) 70:6
https://doi.org/10.1007/s00484-025-03113-0

ORIGINAL PAPER

Divergent occupational heat stress strategies required for Northern and Southern China under climate change

Zhengyuan Liu[1] · Wei Liu[2] · Shuo Wang[3] · Xiuquan Wang[4] · Jinxin Zhu[1] · Dagang Wang[1] · Cong Dong[5] · Guanhui Cheng[6] · Yiwen Mei[1] · Xiaoxing Qi[2]

Received: 15 June 2025 / Revised: 27 August 2025 / Accepted: 29 September 2025 / Published online: 3 January 2026

Abstract

Observable climate change has led to an increase in compound heat events, thereby amplifying the economic impacts of labor heat stress and necessitating intervention strategies. Current research lacks high-resolution precision in projecting future heat stress and quantifying adaptation strategies, which is particularly critical for China given its spatial disparities in climate, workforce distribution, and economic development. This study integrates high-resolution CMIP6 climate models, a Wet-bulb Globe Temperature (WBGT) algorithm, and localized Exposure-response Functions (ERFs) to project heat-induced labor productivity loss across China under the SSP5-8.5 scenario. It systematically analyzes and quantitatively compares the effectiveness of two adaptation strategies (shading and work schedule adjustments) while estimating direct economic losses in outdoor heavy labor industries. This study precisely identifies the thermal stress hotspots categorized as primary (South China: loss rate > 11%, increment 5–7%), secondary (middle-lower Yangtze River: 7–11% loss, 3–5% increment), and tertiary hotspots (Yangtze River Delta & North China Plain: 6–9% loss, 2–4% increment) based on productivity loss magnitudes. Our findings also reveal that optimal strategies diverge north-south along the 33°N: shading dominates in the south and schedule adjustments in the north due to distinct heat patterns, though future climate trends may reduce the efficacy of time shift adjustments nationwide. Additionally, economic loss estimation reveals surging heat-induced losses in agriculture and construction over two decades (annual growth rates of 11.16% and 20.69%, respectively), with combined strategies potentially reducing direct losses by 65–70% in hotspot provinces. These findings enable province- and industry-specific intervention designs considering regional climate variations and strategy effectiveness.

Keywords Climate change · Heat stress · Occupational health · Adaptation

✉ Jinxin Zhu
zhujx29@mail.sysu.edu.cn

Zhengyuan Liu
liuzhy223@mail2.sysu.edu.cn; zhujx29@mail.sysu.edu.cn

Wei Liu
weiliu0608@126.com

Shuo Wang
shuo.s.wang@polyu.edu.hk

Xiuquan Wang
xxwang@upei.ca

Dagang Wang
wangdag@mail.sysu.edu.cn

Cong Dong
cong.dong@gdut.edu.cn

Guanhui Cheng
guanhui.cheng@gdut.edu.cn

Yiwen Mei
meiyw3@mail.sysu.edu.cn

Xiaoxing Qi
uniop@126.com

[1] School of Geography and Planning, Sun Yat-Sen University, Guangzhou, China

[2] School of Government, Sun Yat-Sen University, Guangzhou, China

[3] Department of Land Surveying and Geo-Informatics, The Hong Kong Polytechnic University, Kowloon, Hong Kong

[4] School of Climate Change and Adaptation, University of Prince Edward Island, Charlottetown, Canada

[5] School of Management, Guangdong University of Technology, Guangzhou, China

[6] School of Ecology, Environment and Resources, Guangdong University of Technology, Guangzhou, China

Introduction

Compound humid-heat events have attracted widespread attention due to their profound impacts on socioeconomic systems and human health, with globally observable increases in both frequency and intensity (Li et al. 2020). China stands as one of the hotspot regions for such compound extremes. Nationwide intensification trends in the magnitude and occurrence of compound humid-heat events have been consistently identified across historical observations (Chen 2023; He et al. 2023) and future projections (Chen et al. 2022; Wang et al. 2021), exhibiting faster growth rates compared to extreme heat events (He and Chen 2023). When workers are exposed to heat stress, particularly when surpassing critical temperature thresholds, substantial declines in labor productivity occur through working time loss, thereby generating indirect economic impacts (Ansah et al. 2021). The resultant labor losses from reduced work efficiency have become a globally escalating issue, estimated to cause over 650 billion working-hour losses and nearly $300 billion in annual potential costs (Borg et al. 2021; Zhao et al. 2021; Parsons et al. 2022), with intensified heat-induced labor stress posing significant challenges to China's industrial economy (Chen et al. 2020). Numerous studies have demonstrated pronounced impacts of extreme heat on productivity in primary and secondary industrial sectors (moderate-to-high labor intensity), particularly in developing countries (Sahu et al. 2013; Wyndham 1969; Sheng et al. 2018). Given that China's first and secondary industries still constitute substantial economic proportions with large workforce populations, addressing the cascading impacts of future compound humid-heat events on labor productivity and industrial economies has consequently emerged as a critical scientific challenge.

To address this issue, previous research has primarily focused on three categories: (1) measurement and mechanistic analysis of heat stress (Liljegren et al. 2008; Lemke and Kjellstrom 2012; Foster et al. 2021; Kong and Huber 2022); (2) assessment of labor heat stress impacts on labor productivity and industrial economies (Kjellstrom et al. 2018; Liu et al. 2021; Cheng et al. 2023; Zheng et al. 2023; Sun et al. 2024a, b); (3) strategies for mitigating heat stress(Johansson and Emmanuel 2006; Middel et al. 2021; Parsons et al. 2021; Torbat et al., 2024). Global scholars have proposed over 40 heat stress assessment indices since Haldane's wet-bulb temperature in 1905, evolving to Wallace's wet-bulb dry temperature (WBDT) and relative humidity dry temperature (RHDT) in 2005 (Fanger 1970). Among these, various forms of WBGT remain the most widely used due to their straightforward physical interpretation, comprehensive incorporation of all four environmental factors driving heat stress (temperature, humidity, wind, and radiation), and well-established safety thresholds (Army 2003). Despite limitations such as underestimating thermal stress variations under low airflow and high humidity conditions (Havenith and Fiala 2011), and inadequate reflection of wind's adverse effects in extreme hot-dry environments (Foster et al. 2021), WBGT persists as one of the most extensively applied metrics in climate change and heat stress literature. The energy model developed by Liljegren et al. (2008), which has been rigorously calibrated and validated, is recognized as the optimal method for outdoor WBGT computation. Its simulation of globe temperature accounts for both direct and diffuse solar radiation, ensuring applicability across sunny and cloudy conditions (Lemke and Kjellstrom 2012).

Great efforts have been made to investigate the labor heat stress impacts on labor productivity and industrial economies over the past decades. Early investigations (Kjellstrom et al. 2009a, b) predominantly referenced the ISO7243 standard from the International Organization for Standardization, which defines critical work intensity thresholds based on WBGT to prevent heat-induced declines in work capacity and health risks. Kjellstrom et al. (2018) conceptualized labor productivity as a function of WBGT and work intensity, demonstrating reduced WBGT tolerance limits with increasing labor intensity at constant productivity, and marked productivity declines with rising WBGT under fixed intensity (Kjellstrom et al. 2009b). Building on this framework, Kjellstrom et al. (2018) utilized Sahu et al.'s (2013) comprehensive epidemiological data to derive approximate exposure-response relationships (ERRs) across labor intensities, later refining continuous functions through epidemiological data and ISO 7243 (1989) standards to develop practical ERFs for 200, 300, and 400 W workloads, enabling direct conversion of environmental heat stress (WBGT) into labor productivity loss via generalized normal distribution-based cumulative distribution functions. Subsequent studies predominantly adopted this foundation to establish WBGT-labor loss correlations: Xia et al. (2018) quantified historical heat-related economic losses in Nanjing through input-output modeling; Liu et al. (2021) projected indoor/outdoor industrial losses in China using AMRIO economic models while evaluating air conditioning's mitigation effects.

Strategies to combat heat stress are primarily categorized into two types: engineering control methods and administrative strategies. Engineering control methods include the implementation of sheltering structures (Gu and Zhang 2025), cooling devices (Rowlinson et al. 2014), heat warning systems (Runkle et al. 2019; Shakerian et al. 2021), as well as providing workers with wearable cooling equipment and physiological monitoring devices (Qiao et al. 2022). Administrative strategies encompass the provision of rest facilities and cold water, medical and training support (Song and Zhang 2022; Esfahani et al. 2024), and adjustments

to work and recovery schedules (Chan et al. 2012). Current research on strategies for mitigating occupational heat stress remains relatively limited, primarily focusing on three approaches: cooling interventions (e.g., relocation to air-conditioned/shaded environments), work-rest schedule adjustments, and cooling vest applications (Torbat et al., 2024). Shading interventions and work schedule adjustments are frequently discussed countermeasures. Middel et al. (2021) quantified thermal conditions in shaded versus sun-exposed Arizona summer environments using mobile weather stations, revealing approximately 17 °C reductions in mean radiant temperature under shaded areas. Johansson and Emmanuel (2006) demonstrated nearly 20 °C differences in physiological equivalent temperature between shaded and sun-exposed urban sites in Colombo, Sri Lanka. Li et al. (2016) conducted on-site WBGT measurements for 16 steel reinforcement workers in Beijing during the summer of 2014. The study identified the period of highest heat stress risk for workers as between 14:00 and 15:00, and the lowest risk period as between 07:00 and 09:00 (Li et al. 2016). Parsons et al. (2021) calculated through meteorological reanalysis data that adjusting work schedules by 1–3 h could recover 79% of midday heat-induced productivity losses.

Previous studies exhibit limitations: (1) simplified outdoor WBGT algorithms employed in compound heat assessments often inadequately incorporate critical environmental parameters like atmospheric pressure, solar radiation, and wind speed, with some simplified approaches demonstrating significant flaws; (2) prevailing studies predominantly rely on historical data or CMIP5 (Coupled Model Intercomparison Project Phase 5) projections rather than leveraging the latest 50-km CMIP6 global climate models; (3) adaptation strategy evaluations generally lack large-scale quantitative assessments of expected efficacy, remaining qualitative. To address these gaps, this study employs a comprehensive WBGT algorithm accounting for all environmental factors, integrates a state-of-the-art 50-km CMIP6 model, and evaluates both thermal mitigation effectiveness and economic implications of shading and work schedule adjustments across China. This research aims to assess current and future labor heat stress levels, evaluates adaptation strategies, and quantifies heat-induced productivity losses and industrial economic impacts.

Materials and methods

Estimation of hourly gridded outdoor WBGT

The Liljegren method has been demonstrated as the most effective physical modeling approach for current outdoor WBGT computation (Kong and Huber 2022). It is primarily structured using two independent equations that simulate the energy budgets of natural wet-bulb and black-globe sensors through thermodynamic principles, while considering the effects of air temperature, atmospheric pressure, wind speed, humidity, and solar radiation. This study selected high-resolution (50 km or finer) climate models under SSP585 (Shared Socioeconomic Pathway 5–8.5.5) scenarios from CMIP6 models HadGEM3-GC31-HH (Roberts 2019a) and HadGEM3-GC31-HM datasets (Roberts 2019b). Through validation against observations, the HadGEM3-GC31-HM data was adopted, with temporal divisions for historical (2000–2019) and future (2020–2050) periods. Specifically, multiple reliable historical meteorological datasets (Wu and Gao 2013; Hersbach et al. 2023; Karlsson et al. 2023) were utilized for model validation, with detailed methods and data specifications provided in the Supplementary materials.

The "4+4+4" method for hourly WBGT downscaling (Kjellstrom et al. 2018) disaggregates daily WBGT values into hourly data to better align with diurnal variations in environmental heat stress. This approach partitions daylight hours into three four-hour segments: four hours approximating daily maximum WBGT (WBGTmax) during midday, four hours near daily mean WBGT (WBGTmean) in early morning and evening, and four transitional hours (WBGThalf) between WBGTmean and WBGTmax. According to the 2021 China Report of the Lancet Countdown on Health and Climate Change (Cai et al. 2021), Chinese workers under an eight-hour workday typically operate from 8:00 AM to 5:00 PM with a one-hour break between 12:00 PM and 1:00 PM. This schedule creates distinct heat exposure patterns during working hours: 1 h under WBGTmean conditions, 4 h under WBGThalf conditions, and 3 h under WBGTmax conditions, reflecting the temporal distribution of occupational heat stress exposure throughout the workday.

Realization and quantification of two strategies

This study is the first attempt to quantitatively compare the two important adaptation strategies: shading infrastructure and work schedule modifications. While previous studies have outlined the general efficacy of these strategies (Torbat et al., 2024; Middel et al. 2021; Johansson and Emmanuel 2006; Parsons et al. 2021), most remain confined to policy recommendations without quantitative substantiation. In this study, "shading" is defined as an engineering intervention primarily aimed at reducing the thermal load in work environments by blocking direct solar radiation. Physically, it can take various forms, such as fixed or retractable shade nets, awnings, natural vegetation (e.g., trees) providing shade, and building-generated shadows (Gu and Zhang 2025; Torbat et al., 2024). In the simulation,

the cooling effect of shading was quantified by modifying the WBGT algorithm developed by Liljegren et al. (2008). Specifically, Shading intervention simulation modifies the Liljegren algorithm by setting the downward solar radiation input parameter to 0 W/m², consequently nullifying approximated upward shortwave radiation while preserving calculated upward and downward longwave radiation components (Liljegren et al. 2008). This operation is equivalent to assuming that the shading facilities can block 100% of direct solar radiation, representing an idealized theoretical scenario aimed at evaluating the maximum potential cooling efficiency of shading measures. The physically based framework of Liljegren's model ensures universal applicability across varied conditions, permitting direct code modifications to radiation parameters (Kong and Huber 2022). Finally, it is recognized that implementing shading comprehensively in real-world production environments, particularly in agriculture and construction, faces significant challenges (Torbat et al., 2024). For instance, in field crops such as rice and wheat, canopy operations are difficult to carry out using fixed shading structures. In the construction industry, processes involving work at height, movement of heavy machinery, and continuous pouring (e.g., concrete operations) may not be fully feasible under shaded conditions. The assessment of shading efficiency in this study is conducted under idealized assumptions, representing the theoretical upper limit of this strategy; therefore, our evaluation remains relatively conservative. Practical effectiveness may be compromised by specific environmental conditions, technical limitations, and economic constraints. Work schedule adjustment simulation builds upon Sect. 2.3 methods by reallocating 1–3 work hours originally under WBGTmax conditions to WBGTmean thermal stress forcing, effectively shifting occupational heat exposure from peak solar radiation periods to cooler morning/evening intervals (Table S2).

Estimation of labor losses using erfs

Labor productivity is defined as the ratio between labor output and corresponding labor input over a specific period. It is quantified in macroeconomic terms as output per working hour or per employed individual, while microeconomic measurement considers either product quantity per unit time or labor time expenditure per product unit, thus fundamentally relating to workers' efficiency or temporal resource allocation (Zhang 2011). This operational definition underpins the established relationship between occupational heat stress and productivity loss: under thermal stress exposure, workers require intermittent recovery breaks to maintain health and work continuity, with the proportion of break duration relative to total working time constituting the productivity reduction metric caused by heat stress (Kjellstrom et al. 2018).

The labor loss rate was converted from WBGT using the ERF adjusted according to Chinese occupational health standards (Cheng et al. 2023), with the formula as follows:

$$Loss\ Fraction = \frac{1}{2}\left(1 + erf\left(\frac{WBGT - Prod_{mean}}{\sqrt{2}\ Prod_{sd}}\right)\right) \quad (1)$$

where Loss Fraction represents the percentage of lost working time relative to total work duration. Parameters $Prod_{mean}$ and $Prod_{sd}$ denote functional coefficients for 200 W, 300 W, and 400 W work intensities (Table S1), physically representing internal heat generation during activities, with a detailed parameterization scheme provided in Fig. S5.

Estimation of economic losses

This study collected employment numbers and average wages of employees in agriculture, forestry, animal husbandry, fishery, and construction sectors from 2000 to 2020 using annual statistical yearbook data from China's National Bureau of Statistics website (https://data.stats.gov.cn/easyquery.htmcn=C01). It estimated direct economic losses in labor-intensive industries attributable to occupational heat stress based on labor productivity assessments, and compared provincial-level economic loss outcomes under different adaptation strategies. The calculation methodology proceeded as follows:

$$Economic\ Loss\ (i,j) = \begin{cases} LLP\,(i) \cdot WF\,(i,j) \cdot\ AAW\,(i,j) & ,2000 \leq\ i < 2020 \\ LLP\,(i) \cdot WF\,(2020,j) \cdot\ AAW\,(2020,j) & ,2020 \leq\ i \leq\ 2050 \end{cases} \quad (2)$$

where i denotes the year and j represents different labor-intensive industries (primarily agriculture-related sectors and the construction industry), with LLP signifying the Loss (ratio) of Labor Productivity, WF indicating the Workforce size (population) within each sector, and AAW corresponding to the Average Annual Wage.

Results

WBGT calculation and validation

Figure 1 presents the spatial dynamics of environmental heat stress during the historical validation phase, along with discrepancies between model simulations and observational data. In general, the model data demonstrate reasonable agreement with observational data in spatial distribution. Both datasets identified the primary core regions of heat

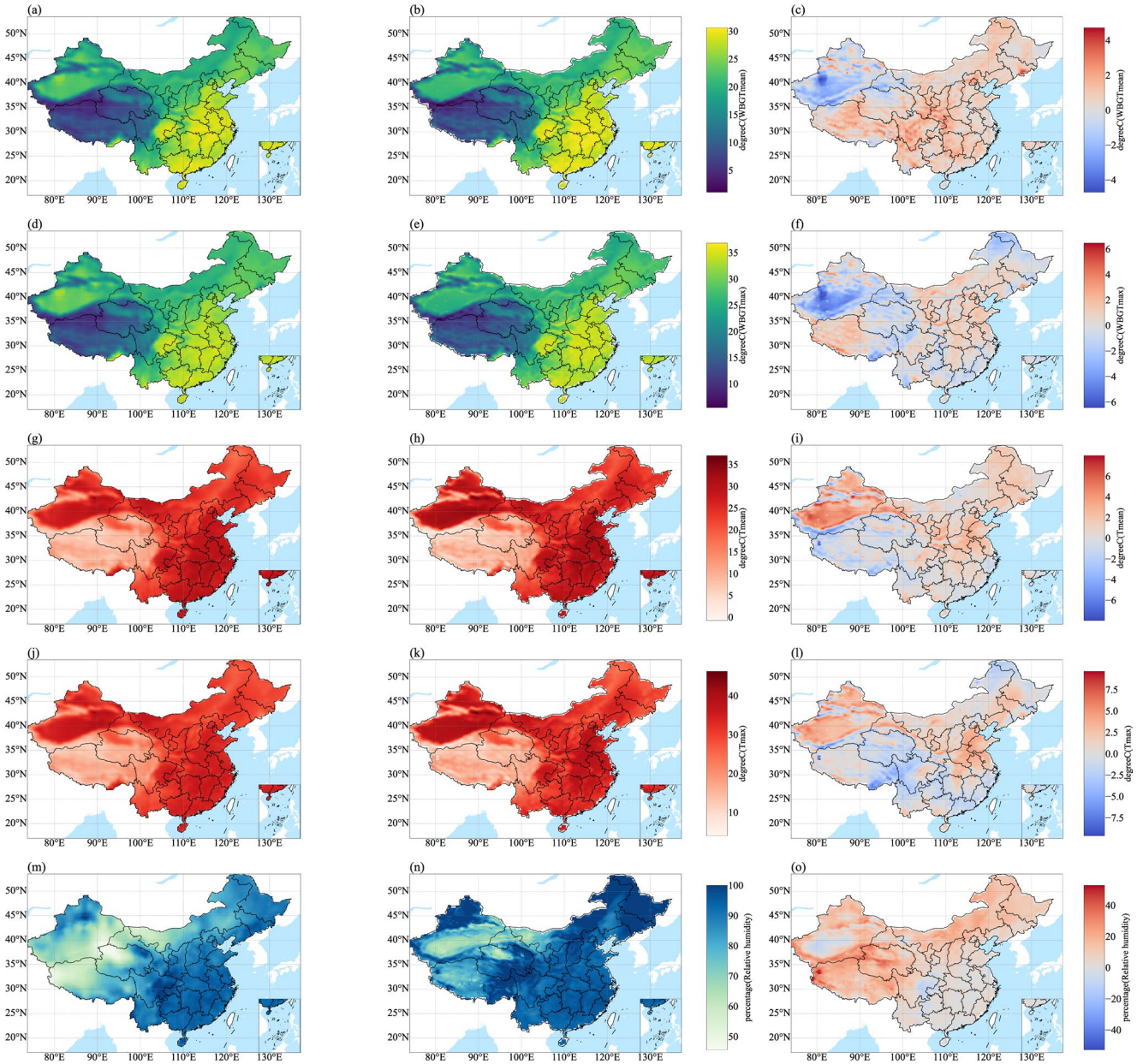

Fig. 1 Validation of spatial patterns of WBGT and key variables (95th percentile) over China (excluding Taiwan Island) during the historical period. Panels (**a**), (**b**), and (**c**) show the observed WBGTmean, model-simulated WBGTmean, and their differences, respectively; panels (**d**), (**e**), and (**f**) present the observed WBGTmax, model-simulated WBGTmax, and their differences; panels (**g**), (**h**), and (**i**) display the observed Tmean, model-simulated Tmean, and their differences; panels (**j**), (**k**), and (**l**) illustrate the observed Tmax, model-simulated Tmax, and their differences; and panels (**m**), (**n**), and (**o**) depict the observed hurs, model-simulated hurs, and their differences

stress over South China, East China, and the eastern Sichuan Basin. In these regions, the 95th percentile of WBGTmean approaches 30 °C, while the 95th percentile of WBGTmax exceeds 35 °C, accompanied by daily relative humidity values at the 95th percentile consistently above 85%. However, the multi-year averaged spatial dynamics (Fig. S6) reveal a slightly distinct pattern, with the absolute core of heat stress centered in the Guangxi-Guangdong-Hainan tri-province region and a secondary core in the eastern Sichuan Basin.

The HadGEM3-GC31-HM model employs an advanced non-hydrostatic dynamical core (NEMO v3.6) and integrates a hybrid turbulence closure scheme in its boundary layer parameterization, which effectively resolves surface-atmosphere energy exchanges. In simulating surface air temperature, the GC31-HM model demonstrates clear improvements. This is primarily attributed to its high-resolution ocean component, which better represents the distribution of sea surface temperature (SST) and sea ice, as well

as its high-resolution atmospheric component, enabling more accurate representation of topography and local circulation. For surface solar radiation, the model achieves more realistic simulations through improved cloud representation, which enhances the realism of SST gradients, convection, and boundary layer processes. Furthermore, owing to better atmospheric circulation responses, refined SST gradients, and more reliable weather system simulations, the model also provides more credible predictions of wind speed, air pressure, and relative humidity (Roberts et al. 2019). While demonstrating notable accuracy in capturing heat stress spatial patterns (limiting hotspot errors to within ± 1 °C), it exhibits systematic biases: a 1–2 °C overestimation in the North China Plain and mid-Yangtze River regions, likely attributable to biases in simulating summer monsoon precipitation. Significant underestimation (2–3 °C) of heat stress occurs in northwestern arid zones, while concurrently overestimating air temperature, reflecting systematic deficiencies in simulating surface radiation balance over dryland ecosystems. The model exhibits systematic relative humidity biases, characterized by underestimation in the high-humidity regions of South China and overestimation in the arid northwest. This discrepancy is primarily attributed to the inadequate representation of subgrid-scale moisture transport in cloud microphysics processes, particularly within the cumulus convection parameterization, leading to systematic errors in moisture flux convergence zones (Liu et al. 2015; Terai et al. 2018; Zhang and Zhang 2022). Given WBGT's higher sensitivity to temperature, humidity errors exert a limited impact (< 5%) on final heat stress assessments.

The model provides a credible projection of future heat stress patterns. In terms of the multi-year average spatial distribution of WBGT, the patterns of daily mean and maximum WBGT are broadly similar and largely follow the latitudinal gradient. South China (including Hainan, Guangdong, and Guangxi) constitutes the highest-risk zone, with WBGTmean ranging between 21.37 °C and 25.76 °C, and WBGTmax between 25.34 °C and 29.25 °C. This region is projected to remain the hottest in China under rising global temperatures, which is consistent with the general understanding. The second-highest zone, located south of the middle-lower Yangtze River (including Hunan, Jiangxi, Zhejiang, and Fujian), shows WBGTmean between 17.54 °C and 20.07 °C, and WBGTmax between 21.54 °C and 24.02 °C. More notably, the spatial pattern of the 95th percentile WBGT differs significantly from the multi-year mean. Extreme heat stress risks in the future are widespread: regardless of latitude, all provinces are expected to experience extreme heat of similar intensity. Specifically, 36% of provinces are projected to have a 95th percentile daily maximum WBGT above 34 °C (high risk), and 72% above 30 °C—including the three northeastern provinces. Moreover, due to weaker monsoon influence in high-latitude regions, the increase in frequency and intensity of extreme heat events will be more pronounced there than in low-latitude coastal provinces. For instance, the increase in the 95th percentile daily maximum temperature in northeastern and northwestern regions is about 1.8 °C, compared to only 1 °C in South China. This represents a major shift from past conditions and implies greater adaptation pressure (Xu et al. 2017; Wang et al. 2023). Furthermore, the spatial distribution of the 95th percentile WBGTmax no longer strictly follows the latitudinal gradient. The highest values are projected in Anhui (35.23 °C), Jiangxi (35.14 °C), and Hunan (34.85 °C). Notably, the top ten provinces all exceed 34 °C, including both traditionally hot southern provinces and those known as China's "Four Furnaces". This suggests that circulation and topography play a more significant role than mere radiative differences in shaping short-term extreme heat events.

Fig. 2 Taylor diagram validation of WBGT and key variables at a provincial level in China (95th Percentile) using the HadGEM3-GC31-HM Model. Panel (**a**) displays the Taylor diagram for the 95th percentile validation of the model output variable WBGTmean during the historical period, while panel (**b**) corresponds to WBGTmax. Panels (**c**), (**d**), and (**e**) represent the input variables Tmean, Tmax, and hurs, respectively

In general, the HadGEM3-GC31-HM model demonstrates good performance in simulating the spatial patterns of WBGT across thermal stress core regions in China, with deviations generally confined within ± 1 °C. Systematic biases in humidity simulations suggest the need for downscaling (Panda et al. 2022) or the integration of high-resolution land surface models (Sun et al. 2024a, b; Birylo et al. 2025) to enhance the representation of land-atmosphere interactions.

The normalized standard deviation (NSD), normalized mean square error (NMSE), and correlation coefficient (R) were employed as quantitative metrics, with Taylor diagrams serving as visual representations. These metrics were used to demonstrate the validation performance of key variables across both temporal and spatial patterns at national and provincial levels. National-scale results (Fig. S3) reveal that the spatio-temporal patterns of WBGT and temperature variables exhibited R consistently above 0.97, with NMSE < 0.25 and NSD ranging between 1.0 and 1.2. For relative humidity, spatial validation achieved R exceeding 0.7 with NMSE < 0.75. Provincial-level validation results (Fig. S7) demonstrate that all provinces maintain WBGT and temperature time-series R above 0.9, accompanied by NMSE < 0.5. Figure 2 presents the model validation performance in WBGT outputs and key inputs (95th percentile). Regarding the WBGTmean metric, most provinces exhibit $R > 0.85$, NSD of 0.9–1.1, and NMSE < 1.5, indicating that

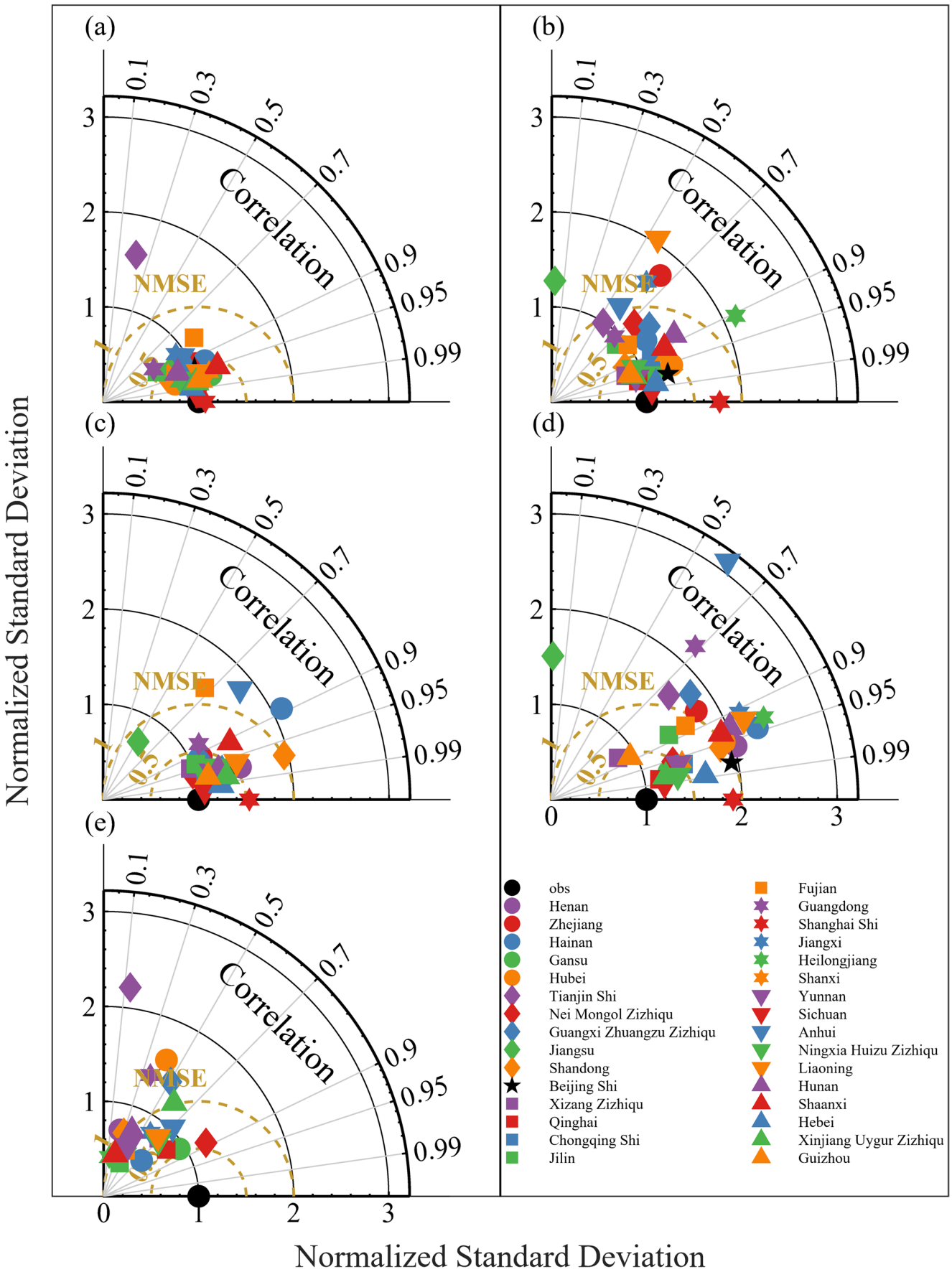
(a)
(b)
(c)
(d)
(e)
Correlation
NMSE
0.1
0.3
0.5
0.7
0.9
0.95
0.99
Normalized Standard Deviation
Normalized Standard Deviation
obs
Henan
Zhejiang
Hainan
Gansu
Hubei
Tianjin Shi
Nei Mongol Zizhiqu
Guangxi Zhuangzu Zizhiqu
Jiangsu
Shandong
Beijing Shi
Xizang Zizhiqu
Qinghai
Chongqing Shi
Jilin
Fujian
Guangdong
Shanghai Shi
Jiangxi
Heilongjiang
Shanxi
Yunnan
Sichuan
Anhui
Ningxia Huizu Zizhiqu
Liaoning
Hunan
Shaanxi
Hebei
Xinjiang Uygur Zizhiqu
Guizhou

the model effectively captures interannual variations in heat stress. Outliers such as Tianjin and Shanghai show $R<0.7$ with NMSE>2, likely attributable to sampling biases induced by sparse regional grid coverage, resulting in inadequate representation of land-sea breeze interactions and urban heat island effects. For the WBGTmax metric, inland provinces (e.g., Xinjiang, Sichuan) demonstrate $R>0.8$ and NSD of 1.0–1.2, reflecting reasonable reproduction of extreme events.

The input variables Tmean and Tmax demonstrate $R>0.9$, NMSE<0.75, and NSD of 1.0–1.5 in most provinces. Validation performance in inland arid regions (e.g., Gansu, Xinjiang) is markedly superior to coastal areas, with $R>0.95$ and NMSE<0.6. Outlier analysis (Fig. 2c and d) reveals that Jiangsu Province concurrently exhibits low NSD and reduced R values, indicating systematic underestimation of spatial thermal heterogeneity in the model. Recent CMIP6-based studies on heat extremes have demonstrated that urbanization in the Yangtze River Delta, with its unique circulation patterns and heterogeneous underlying surfaces, has led to heatwave events more severe than those simulated by CMIP6 models (Sun and Hu 2023; Wei et al. 2024; Zhang et al. 2024). The model's superior performance in simulating extreme temperature and precipitation events has been validated in previous studies, even surpassing many CMIP5 regional climate models. (Wang et al. 2025; Li et al. 2022; Eman et al. 2024) Generally, the HadGEM3-GC31-HM model demonstrates reliable simulation capabilities for the WBGT (95th percentile) and achieves robust reconstruction of spatial patterns of environmental heat stress across China, thereby providing a solid foundation for subsequent assessments of regional labor productivity losses.

Spatiotemporal evolution of labor loss rates

Figure 3 illustrates the spatiotemporal evolution characteristics of the LLP distribution in China under different labor intensity levels. Under low-intensity labor conditions (200 W), current LLP generally remains below 10%, with most regions in North China, East China, Central China, and South China maintaining approximately 5% levels, while localized areas in South China reach 10%. Projected future increments (Δ) are typically less than 3%, though high-value zones (Δ>4%) emerge in coastal South China (Guangdong, Guangxi, and Hainan) and the Sichuan Basin. For moderate-intensity labor (300 W), current hotspot

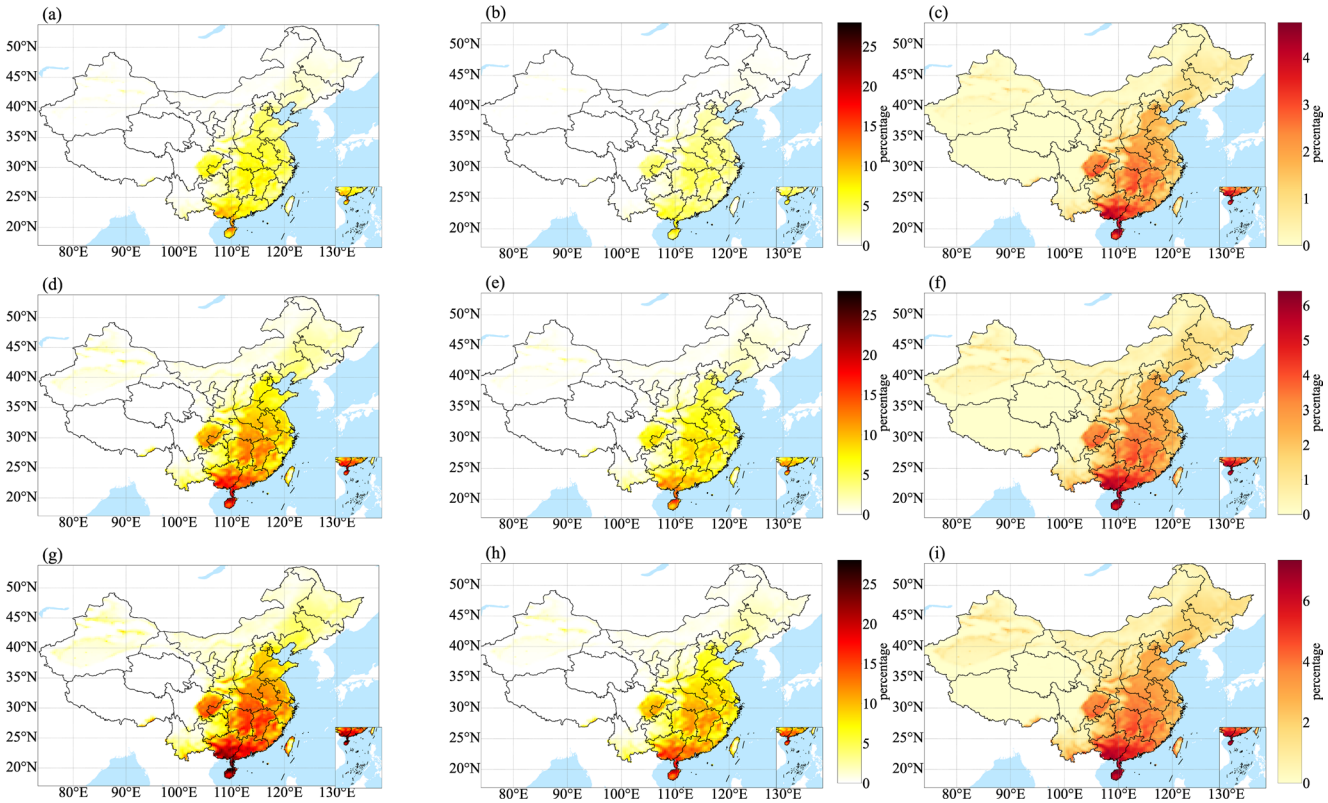

Fig. 3 Historical vs. Future LLP in China under Varied Work Intensities and Hotspot Classification. Panels (**a**), (**b**), and (**c**) illustrate the projected future values, historical simulated values, and their differences (increments in future periods relative to historical periods) for LLP under 200w labor intensity, respectively. Panels (**d**), (**e**), and (**f**) present comparable analyses for 300w labor intensity scenarios. Panels (**g**), (**h**), and (**i**) display equivalent datasets for 400w labor intensity conditions, showing projected future values, historical simulations, and incremental differences between the two temporal phases

regions (LLP > 10%) are concentrated in the middle-lower Yangtze River basin (Hubei, Hunan, and Jiangxi) and coastal South China. With the projected significant reduction in precipitation and intensified drought conditions in this region (Huang et al. 2024), the core area of future increments (Δ > 4%) extends northwestward to the Sichuan Basin.

High-intensity labor (400 W) exhibits a three-tiered hotspot stratification: Tier 1 hotspots (Guangdong, Guangxi, and Hainan) demonstrate current LLP > 11% with future increments Δ5–7%; Tier 2 hotspots (Hubei, Hunan, Jiangxi, and eastern Sichuan) show current LLP of 7–11% coupled with Δ3–5%; Tier 3 hotspots (Yangtze River Delta, and North China Plain) present current LLP of 6–9% corresponding to Δ2–4%. Although non-hotspot regions (Northeast and Northwest) exhibit increments Δ < 2%, their economic risks stemming from higher agricultural dependence still require incorporation into adaptive strategies. Analysis of the loss function reveals a nonlinear relationship between labor intensity and heat stress susceptibility. Mechanistic analysis reveals that: (1) Tier 1 hotspots are governed by tropical marine climates where annual mean relative humidity > 80% elevates WBGTmax beyond 34 °C. Figure 1 indicates a 15% bias in HadGEM3-GC31-HM's simulation of extreme humidity, potentially underestimating thermal risks in South China; (2) For Tier 2 hotspots, the Sichuan Basin experiences topographic heat-trapping effects compounded by prolonged subtropical high-induced droughts, where projected 10–20% precipitation reduction decreases surface evapotranspiration, while intensified solar radiation drives WBGTmax escalation; (3) Tier 3 hotspots face synergistic urbanization (30% projected urban land expansion), amplifying compound "heatwave-high humidity" event frequency.

Figure 4 illustrates LLP variations under different adaptation strategies during the future period (2020–2050) for medium-low intensity labor (200 W and 300 W). Shading adjustment demonstrates high efficacy in southern regions with loss reductions of 50–60% versus ~40% in northern areas, attributable to stronger solar radiation attenuation through shading in radiation-intensive southern zones. Conversely, work schedule adjustment (3 h) exhibits enhanced performance in northern China (50–70% loss reduction) compared to southern provinces (~40%), driven by northern China's greater diurnal temperature range (> 10 °C daily amplitude) versus persistent nocturnal humidity in southern regions that decouples wet-bulb temperature depression from ambient air temperature reduction. This spatial

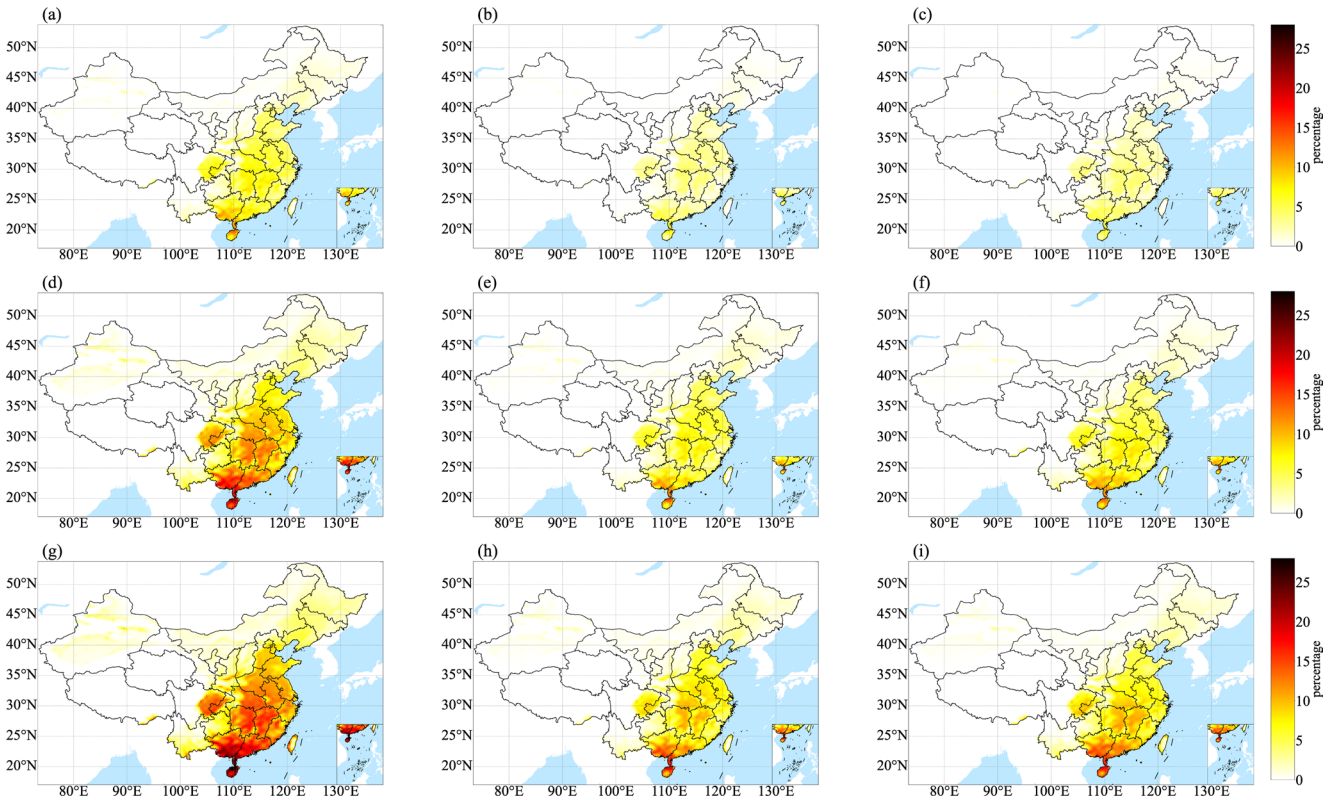

Fig. 4 Comparative Effectiveness of Shading and 3 h Work Shift Adjustment Strategies on Future LLP in China under Varied Work Intensities. Panels (**a**)-(**c**) illustrate spatial distributions of LLP under non-intervention, shading adjustment, and 3 h work shift adjustment strategies respectively for 200 W labor intensity. Similarly, Panels (**d**)-(**f**) present comparable results for 300 W intensity, while Panels (**g**)-(**i**) display outcomes for 400 W intensity under identical intervention strategies

divergence stems from thermodynamic disparities: shading directly mitigates radiative heat transfer (dominant in southern energy budgets) while work schedule shifts leverage favorable thermal inertia conditions (pronounced in northern dry climates).

Regarding the north-south divergence in intervention efficacy for high-intensity labor (400 W): (1) Under non-intervention scenario, Tier 1 hotspots exhibit LLP > 15%, Tier 2 hotspots > 10.5%, and Tier 3 hotspots > 7%; (2) Shading adjustment reduce loss rates by 40% on average in hotspot provinces, exemplified by Hainan's decrease from 21.74% to 13.27% and Hebei's reduction from 5.48% to 3.14%, with comparable north-south efficacy under 400 W labor intensity despite shading's superior performance in southern regions at 200/300 W levels, likely attributable to reduced sensitivity of heat stress indicators to solar radiation during high-intensity exertion; (3) Work schedule adjustment (3 h) achieves ~ 50% loss reduction in northern hotspots (e.g., Shandong's decline from 8.37% to 4.58%) versus merely 33% in southern counterparts (e.g., Guangdong's decrease from 16.17% to 10.69%), maintaining significant north-south performance disparity despite shading's diminished regional differentiation at 400 W intensity, as further analyzed and visually demonstrated in Fig. 5.

The red base map in Fig. 5 illustrates the provincial-level distribution of future high-intensity (400w) LLP increments (Δ). The regions with the largest increments are South China (e.g., Guangdong with 4.79%Δ, Hainan with 5.63%Δ), followed by the middle reaches of the Yangtze River (Hunan with 3.85%Δ), reflecting the intensified synergistic effect of heat and humidity. Northern regions show lower increments (Hebei 1.99%Δ, Jilin 1.44%Δ), yet their high economic vulnerability (strong agricultural dependence) necessitates targeted interventions. The histogram of Fig. 5 shows significant differences in optimal strategy types between southern and northern provinces, roughly divided by the 33°N. This

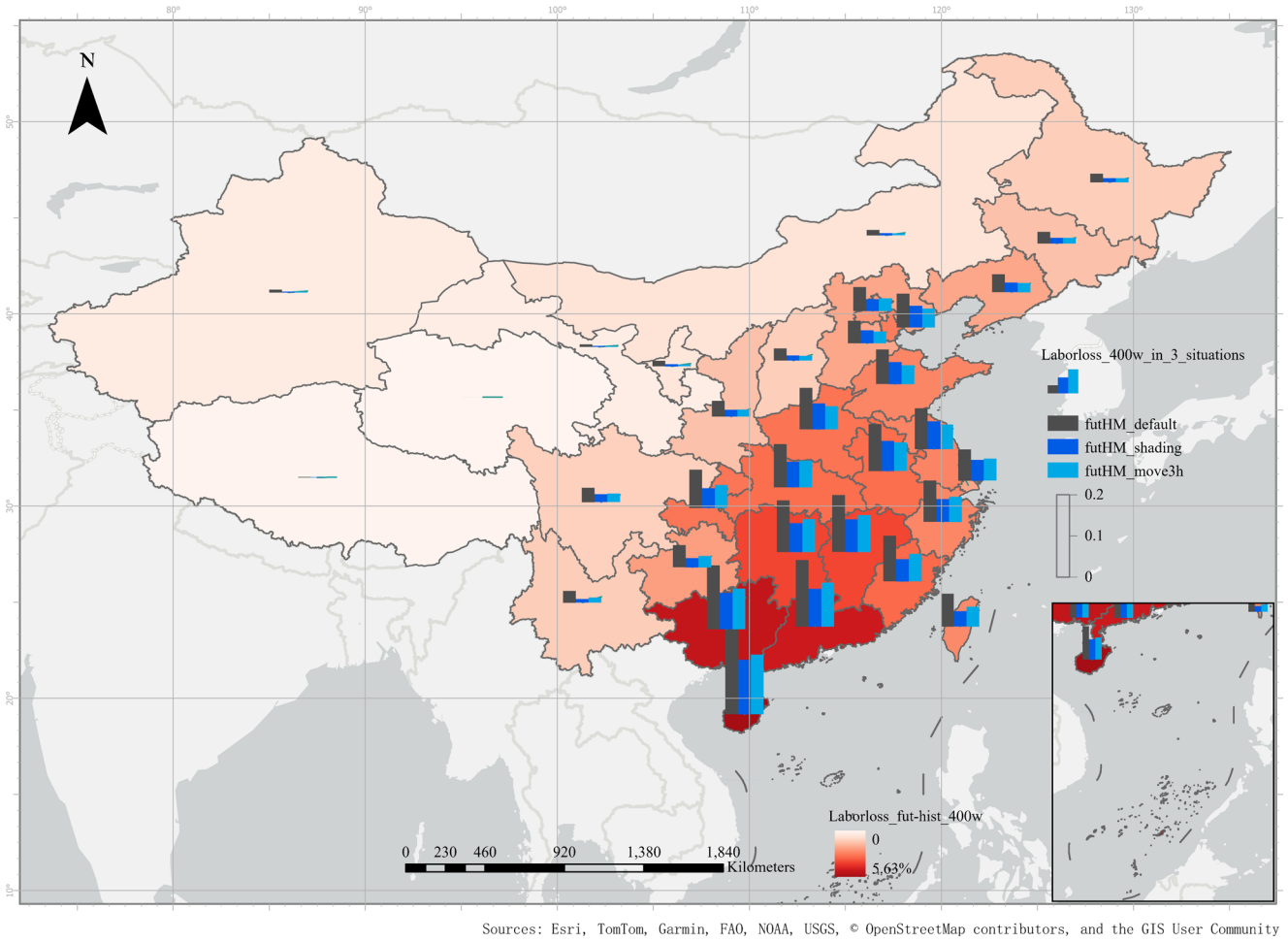

Fig. 5 North-South Disparity in Labor Loss Reduction under Shading and 3 h Work Shift Strategies for High-Intensity Work (400 W) in China. The red-shaded base map (excluding Hong Kong and Macao) uses color gradients to represent the incremental labor loss rates of corresponding industries under 400 W labor intensity during the future period (relative to historical periods). The heights of the gray, dark blue, and light blue bars in the histogram correspond to: future labor productivity losses under no interventions, labor productivity losses under shading adjustment, and labor productivity losses under the 3 h working adjustment strategies, respectively

allows comparative analysis of strategy effects in typical southern and northern provinces. Guangdong Province is selected as a southern case due to its dense and concentrated population, large economic output, and subtropical monsoon climate, where industrial economies suffer severe heat stress impacts. Under a non-intervention scenario, Guangdong's LLP reaches 16.17%. Implementing ideal shading strategies could reduce this to 9.20% (43.10% decrease), while adopting a 3 h work shift adjustment would lower it to 10.69% (33.89% decrease). The shading adjustment outperforms work schedule adjustments due to Guangdong's proximity to the Tropic of Cancer, where daytime solar elevation angles exceed 80° in summer, enabling an effective reduction of direct radiation through shading. Henan Province serves as a northern case due to its status as a major agricultural and populous province with climate-sensitive industries. Without interventions, its LLP is 10.06%. Ideal shading reduces this to 6.32% (37.18% decrease), while work schedule adjustment (3 h) lowers it to 5.62% (44.14% decrease). Northern provinces benefit more from work schedule adjustments because of larger diurnal temperature ranges (6–8 °C lower morning temperatures than daytime).

Considering future climate change impacts, strategies may require adjustments. Enhanced East Asian summer monsoon will increase southern moisture transport, with models predicting 5–10% relative humidity increases. This further reduces work schedule adjustment effectiveness, elevating shading strategies' importance. Northern regions may face intensified aridity, with 10–15% precipitation reductions in North China and increased dry heat events, potentially shortening morning work windows. Dynamic adjustments based on medium-range weather forecasts will be necessary. Climate change will first impact outdoor labor-intensive industries (agriculture, forestry, construction). Combining LLP with employment/wage data to estimate heat stress-related economic losses in sensitive sectors is critical and provides valuable insights.

Valuation of direct economic losses in heavy labor industries

Figure 6 presents projected heat stress-induced economic loss estimates and adaptation potential for agriculture-related sectors (including agriculture, forestry, animal husbandry, and fishery) and the construction sector under future climate conditions. For the agriculture-related sectors shown in Fig. 6(a), the top five provincial administrative regions with direct economic losses (orange segments) under the non-intervention scenario are Guangxi, Guangdong, Shandong, Henan, and Hunan, where maximum losses reach 2513.76 billion yuan (Guangxi) versus 1687.68 billion yuan (Hunan), representing a 30% gap, with provincial averages at 2192.92 billion yuan. These losses primarily stem from intensive agricultural labor under summer heatwaves, particularly affecting southern provinces with daily WBGT exceeding 32 °C during peak farming seasons, compounded by dense agricultural workforce concentrations (e.g., >40% agricultural population in Guangxi). Though Shandong and Henan fall outside core heat stress zones, their substantial agricultural populations warrant attention. Combined shading and 3-hour work adjustments achieve a 66% average loss reduction in hotspot provinces (e.g., Guangxi's loss decreased to 778.20 billion yuan). Shading lowers field radiant temperatures by approximately 3 °C; however, its application is limited by crop type. It is more feasible in cash crop plantations (e.g., orchards, tea gardens) or seedling nurseries, yet difficult to implement in open-field crops. Moreover, in some agricultural settings where shading is easily achievable (e.g., greenhouses), it may create even more extreme hot and humid environments compared to the exterior.

Figure 6(b) demonstrates the spatial pattern of heat stress-induced direct economic losses and adaptation bottlenecks in the construction sector under a non-intervention scenario, exhibiting a tiered distribution. Specifically, Jiangsu (1895.86 billion yuan) surpasses Guangdong (1333.78 billion yuan), Fujian (1136.48 billion yuan), and Zhejiang (1116.29 billion yuan), while Hunan (526.52 billion yuan) shows comparable losses to subsequent provinces (Henan, Shandong), with the top four provinces averaging 1370.60 billion yuan losses. This pattern reflects compounded effects of construction intensity and extreme heat (WBGTmax > 34 °C) in urbanized hotspots (e.g., Yangtze River Delta, Pearl River Delta), driven by dense construction workforce concentrations (e.g., Jiangsu's 8.55 million construction workers in 2020) and heatwave-induced rush work due to rigid project timelines. Although ideal adaptation measures could recover ~ 60% of losses (e.g., Jiangsu's reduction to 694.28 billion yuan), implementation faces dual constraints. Both sectoral analyses highlight that current intervention efficacy assessments must account for operational rigidities inherent to labor-intensive industries.

Figure 7(a) illustrates historical growth trends (2000–2019) of direct heat stress-induced economic losses in agriculture-related sectors and the construction sector. Aggregate data reveal that agriculture-related sector losses surged from 96.78 billion yuan in 2000 to 610.96 billion yuan in 2019, representing a 531.29% cumulative increase (11.16% annualized growth rate), while the construction sector losses escalated from 8.98 billion yuan to 268.81 billion yuan, marking a 2893.42% rise (20.69% annualized growth rate). Sectoral analysis indicates that agriculture-related industries (primary sector) persistently dominated labor-intensive industry losses, though their share declined

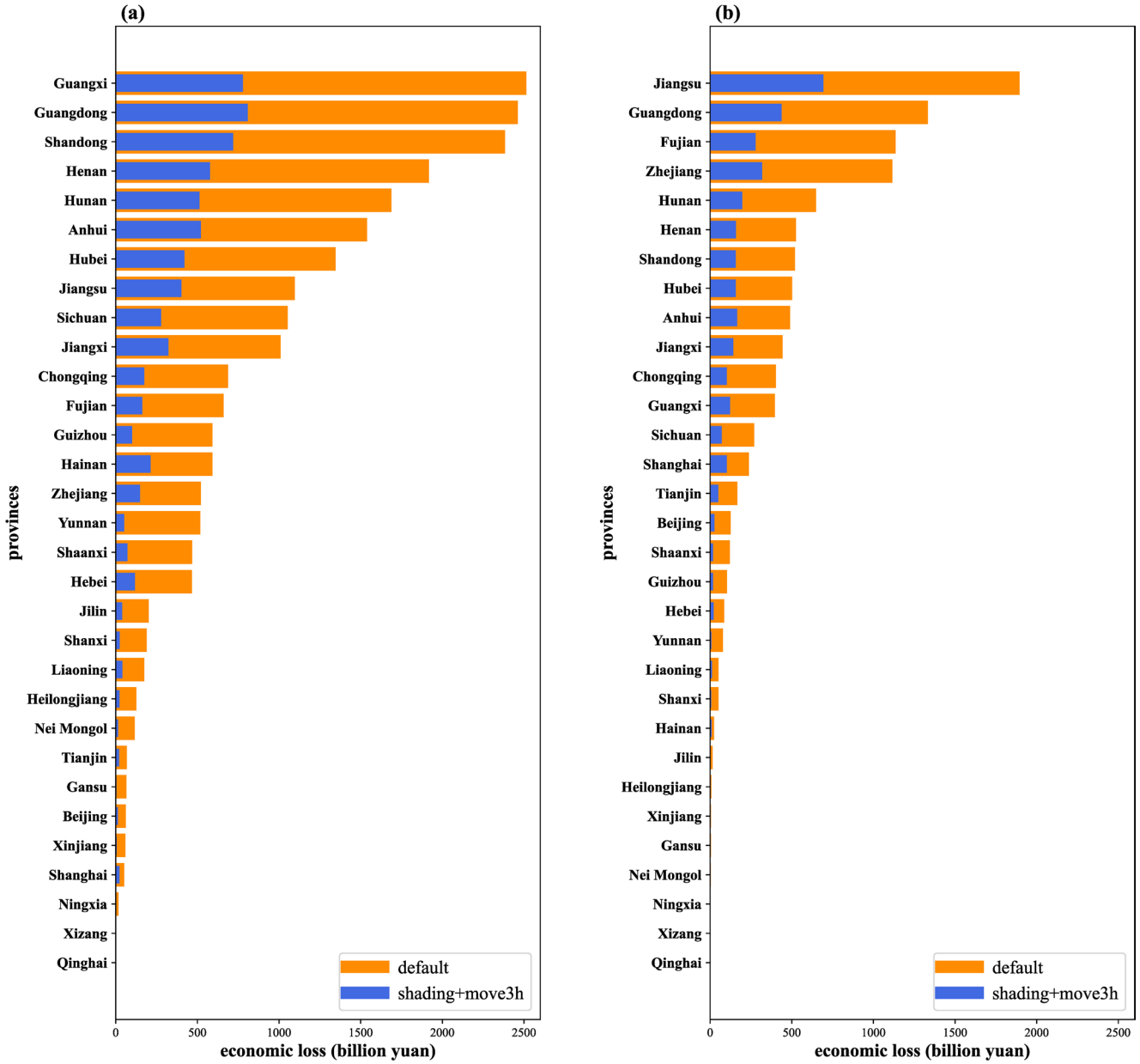

Fig. 6 Economic Loss Assessment of Heat Stress on Agriculture and Construction Sectors in China: Effectiveness of Adaptation Strategies. Panel (**a**) illustrates estimated direct economic losses incurred by the agriculture-related sectors specifically attributable to heat stress exposure. Panel (**b**) presents analogous loss projections for the construction industry under equivalent thermal stress conditions. Orange-colored segments represent loss magnitudes under the baseline scenario with a non-intervention strategy, while blue-colored segments represent loss levels achievable under optimized countermeasure conditions (simultaneous implementation of shaded work environments and 3 h work shift adjustments across all heavy labor positions). The x-axis quantifies economic losses in billion CNY units, with the y-axis displaying the provincial-level administrative divisions within China (excluding Hong Kong, Macao, and Taiwan)

significantly from 91.51% (2000) to 69.45% (2019). Conversely, the construction sector losses accounted for 30.55% of total labor-intensive industry losses by 2019, demonstrating exceptional growth momentum. Figure 7(b) demonstrates adaptation potential under multiple intervention scenarios for future heat stress-induced economic losses in agriculture-related sectors across selected hotspot provinces. Under non-intervention scenario: Guangdong's high projected losses (2461.74 billion yuan) stem from intensifying humid-heat climates (summer WBGTmax up to 34 °C); Shandong (2383.44 billion yuan) reflects its dominant agricultural output value nationally; Hunan's elevated losses (1687.68 billion yuan) originate from exacerbated midsummer droughts in critical rice-growing areas under strengthened subtropical high-pressure systems; Jiangsu's agricultural losses (1096.65 billion yuan) likely

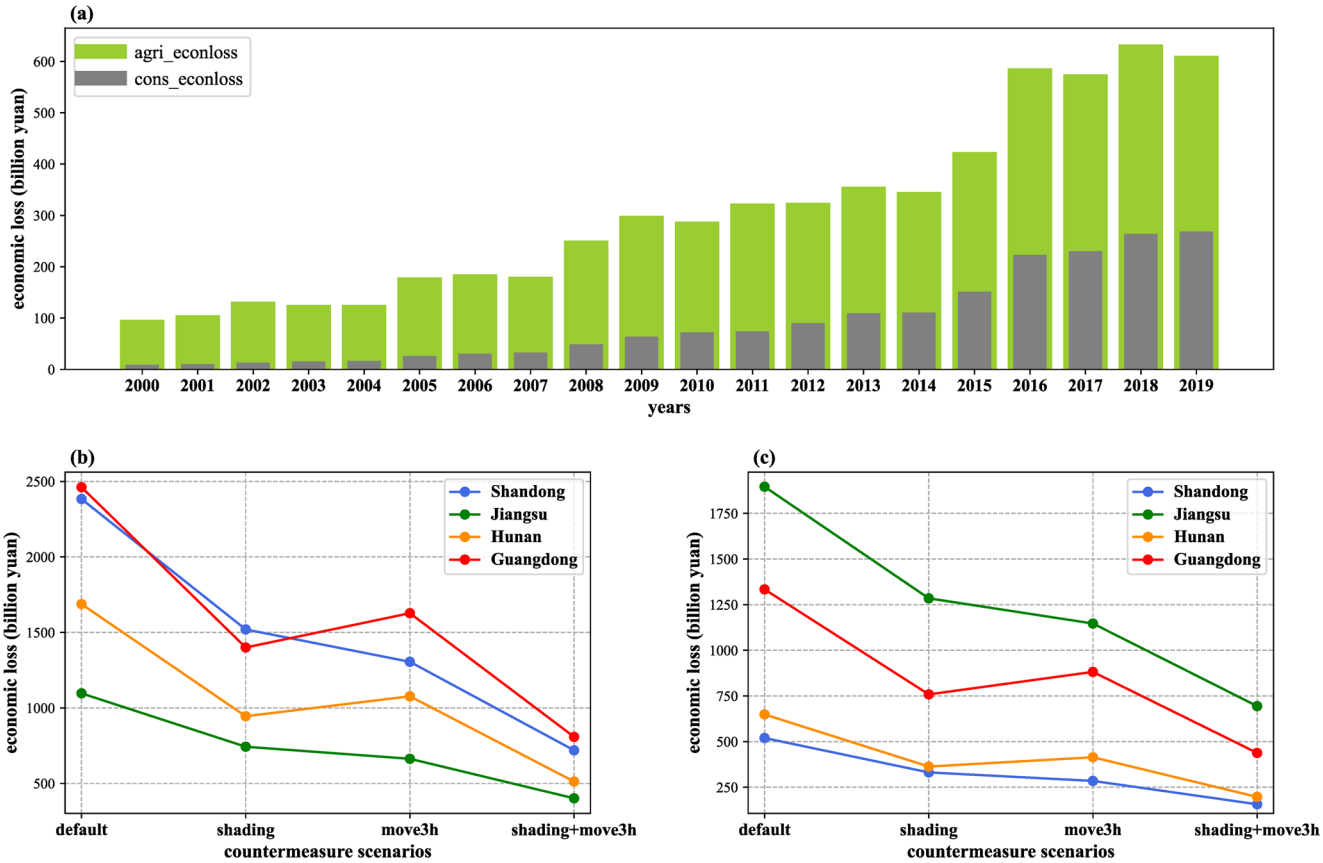

Fig. 7 Spatiotemporal Evolution and Sector-Region Specific Intervention of Heat Stress-Induced Economic Losses in China. (**a**) The figure illustrates the estimated direct economic losses incurred by the agriculture-related sectors as well as the construction industry due to heat stress on a yearly basis during the historical period. The horizontal axis represents the years of the historical period, and the vertical axis indicates the economic losses, measured in billion CNY. (**b**) and (**c**) respectively present the estimated direct economic losses for the agriculture-related sectors and the construction industry in four typical provinces of key regions during the future period, directly caused by heat stress. The horizontal axes represent different countermeasure scenarios: non-intervention, shading adjustment, 3 h work shift adjustment strategies, and the combined application of shading and three-hour work shift adjustment countermeasure. The vertical axes indicate the economic losses, measured in billion CNY

relate to high greenhouse farming ratios with inadequate ventilation. For intervention outcomes: standalone shading reduces Guangdong's losses to 1400.25 billion yuan (43.12% reduction) and Shandong's to 1519.85 billion yuan (36.23% decrease), while work schedule adjustment (3 h) alone decreases Shandong's losses to 1305.55 billion yuan (45.22% reduction) versus Guangdong's 1627.25 billion yuan (33.90% decrease). Combined interventions further reduce provincial losses (e.g., Guangdong to 808.33 billion yuan, Shandong to 719.31 billion yuan), though residual risks persist (30–35% of baseline losses).

Figure 7(c) demonstrates the adaptation potential of multiple countermeasure scenarios for economic losses in the construction industry of selected hotspot provinces during the future period. Under the non-intervention scenario, Guangdong Province is projected to incur losses of 1333.78 billion yuan and Jiangsu Province 1895.86 billion yuan, with annual averages exceeding 40 billion yuan. Despite both provinces having rapid urbanization and substantial construction industries (Guangdong's construction workforce: 3.42 million in 2020; Jiangsu's: 8.55 million), Guangdong's elevated losses primarily stem from intensifying climate stress, whereas Jiangsu's result from its exceptionally large construction workforce. Shandong (519.59 billion yuan) and Hunan (648.94 billion yuan) exhibit relatively smaller construction industries. Implementing singular strategies yields varying reductions: shading adjustment decreases Guangdong's losses to 758.65 billion yuan (−43.12%) and Jiangsu's to 1284.71 billion yuan (−32.24%), while work schedule adjustment (3 h) reduces Jiangsu's losses to 1146.61 billion yuan (−39.52%) and Guangdong's to 881.64 billion yuan (−33.90%). The optimal combined implementation achieves maximum recovery, reducing losses to 437.95 billion yuan in Guangdong and 694.28 billion yuan in Jiangsu. However, practical bottlenecks exist in the implementation of these strategies.

In the agricultural sector, the effectiveness of shading strategies exhibits significant sectoral and regional heterogeneity. For example, canopy management in field crops such as rice and wheat is hardly compatible with fixed shading structures. In the construction industry, while shading measures (e.g., temporary canopies) may be feasible for certain ground-level operations, it is unrealistic to completely avoid outdoor work during high-temperature periods due to engineering safety standards and process requirements. Therefore, although models indicate substantial shading potential, its actual penetration and effectiveness on construction sites are expected to be lower than theoretical values. This suggests that future adaptation planning must integrate technological substitutions (e.g., mechanization, remote operation via drones) and management adjustments (e.g., flexible working hours, mandatory rest periods), rather than relying solely on singular shading engineering measures.

This study inevitably has several limitations: (1) it did not account for feedback effects on exposure from future labor force transfers (e.g., increased agricultural mechanization rate) and policy interventions (e.g., carbon emission reduction), necessitating future coupling with socioeconomic scenarios to refine parameter settings; (2) the assumption of strategy implementation was overly idealized, neglecting real-world constraints such as delayed infrastructure popularization in rural areas; (3) it did not assess the compounding effects of compound climate hazards such as rainstorms/typhoons.

Discussion and conclusion

This study utilizes 50-km resolution CMIP6 climate model data to project China's heat stress risk distribution under the SSP585 scenario through a validated WBGT algorithm, calculates labor productivity loss using ERF calibrated with Chinese occupational health standards, evaluates the effectiveness of primary adaptation strategies, and estimates direct economic losses in outdoor heavy labor industries. The research innovations focus on: achieving provincial-level precision in labor loss assessment through high-resolution climate data and localized ERF; systematically comparing shading and work schedule adjustment strategies while analyzing their implementation implications shaped by notable north-south effectiveness disparities; quantifying future direct economic losses using robust statistical frameworks to inform policy formulation and cost-benefit analysis.

This study delineates hotspot regions through identifying future heat stress and labor productivity loss risks, revealing distinct patterns across labor intensities: low-intensity work (200 W) currently exhibits < 10% productivity loss nationwide, with future core increase zones projected in coastal South China and the Sichuan Basin; medium-intensity labor (300 W) demonstrates current hotspots concentrated in the middle-lower Yangtze River basin and coastal South China, while future loss increments shift toward the Sichuan Basin experiencing 20% precipitation reduction; high-intensity work (400 W) forms a tri-level hotspot hierarchy - primary hotspots (Guangdong, Guangxi, Hainan) show current losses > 11% with 5–7% future increases driven by high-humidity environments (RH > 80%) and intensifying typhoons, secondary hotspots (Hubei, Hunan, Jiangxi, eastern Sichuan) associate with terrain-induced heat stagnation and aggravated aridity, while tertiary hotspots (Yangtze River Delta and North China Plain) face synergistic urbanization (30% projected urban land expansion) and greenhouse effects, amplifying compound "heatwave-haze-high humidity" event frequency.

This study reveals significant north-south divergence in heat stress mitigation effectiveness across China, with shading strategies demonstrating superior performance in southern regions (~20% greater efficacy) compared to work schedule adjustments preferred in northern areas. This spatial pattern primarily stems from southern China's higher solar altitude and persistent nocturnal humidity (RH > 80%) that diminish the benefits of temporal adjustments, contrasting with northern regions' pronounced diurnal temperature variations enabling 5–7 °C morning WBGT reductions. While shading achieves comparable effectiveness (~40% loss reduction) for high-intensity labor (400 W) nationwide, work schedule adjustments maintain marked north-south disparities. Primary hotspots (Guangdong and Hainan) require prioritized interventions against humidity-heat synergism, exhibiting WBGT humidity sensitivity > 2 °C/10%RH under moist conditions versus nearly linear temperature-WBGT correlations in arid northern climates. The optimal strategy boundary aligns with the 33°N, reflecting southern humidity-dominated versus northern temperature-driven heat stress mechanisms. Model projections indicate worsening regional divergence: southern humidity increases (5–10%) and northern warming coupled with aridification will jointly degrade temporal adjustment efficacy, reinforcing the necessity for geographically differentiated adaptation frameworks.

This study projects substantial divergence and shared patterns in heat stress-induced economic losses across China's agriculture-related industries and construction sector under climate change: Without intervention, the top five provinces face average direct economic losses of 219.292 billion yuan annually per province in agriculture-related industries, primarily attributable to high-humidity zones (e.g., Guangdong, Guangxi) combined with dense agricultural populations (e.g., Guangxi, Shandong), while combined

shading and temporal adjustment strategies could achieve 66% loss recovery. Construction sector losses exhibit tiered provincial distribution, with Jiangsu (189.586 billion yuan) ranking highest due to concentrated workforce and frequent extreme heat events, where optimal strategies could mitigate 60% of losses. Future strategy combination analysis demonstrates limited efficacy of single interventions with significant regional disparities between northern and southern provinces, whereas theoretically optimized dual-strategy implementation could reduce direct economic losses by 65–70% under ideal conditions.

Supplementary Information The online version contains supplementary material available at https://doi.org/10.1007/s00484-025-03113-0.

Acknowledgements This research was funded by the Guangzhou Basic and Applied Basic Research Foundation (Grant No. 2025A04J5097), the National Natural Science Foundation of China (Grant No. 42301021), and the Natural Science Foundation of Guangdong Province (Grant No. 2023A1515012528). We acknowledge and thank the climate modeling groups in the Coupled Model Intercomparison Project for generating their model outputs and making them available.

Author contributions J.X. Zhu initiated the study and contributed to research design. Z.Y. Liu cleaned the data, performed analyses, and write the first draft of the manuscript. W. Liu, S. Wang, X.Q. Wang, D.G. Wang, D. Cong, G.H. Cheng, Y.W. Mei, and X.X. Qi provided valuable suggestions and revised the paper. All authors have read the final manuscript and approved the submission.

Data availability Data used in this paper is freely available at Mendeley Data (DOI: https://doi.org/10.17632/cd2hhwh6sy.2).

Declarations

Declaration of competing interest The authors declare that they have no known competing financial interests or personal relationships that could have appeared to influence the work reported in this paper.

References

Ansah EW, Ankomah-Appiah E, Amoadu M, Sarfo JO (2021) Climate change, health and safety of workers in developing economies: a scoping review. The Journal of Climate Change and Health 3:100034. https://doi.org/10.1016/j.joclim.2021.100034

Army U (2003) Heat stress control and heat casualty management. Department Army Air Force Tech Bull TBMED507/AFPAM:48–152

Birylo M, Błaszczak-Bąk W, Suchocki C (2025) Application of GLDAS models and ALS point clouds in assessing the impact of modified evapotranspiration on the water budget. Water Res 123746. https://doi.org/10.1016/j.watres.2025.123746

Borg MA, Xiang J, Anikeeva O, Pisaniello D, Hansen A, Zander K, Dear Keith, Sim Malcolm R., Bi P (2021) Occupational heat stress and economic burden: a review of global evidence. Environ Res 195:110781. https://doi.org/10.1016/j.envres.2021.110781

Cai W, Zhang C, Zhang S, Ai S, Bai Y, Bao J, Gong P (2021) The 2021 China report of the lancet countdown on health and climate change: seizing the window of opportunity. Lancet Public Health 6(12):e932–e947. https://doi.org/10.1016/S2468-2667(21)00209-7

Chan AP, Yi W, Wong DP, Yam MC, Chan DW (2012) Determining an optimal recovery time for construction rebar workers after working to exhaustion in a hot and humid environment. Build Environ 58:163–171. https://doi.org/10.1016/j.buildenv.2012.07.006

Chen X (2023) Significant increases in wet nighttime and daytime–nighttime compound heat waves in China from 1961 to 2020. Atmosphere 14(1):178. https://doi.org/10.3390/atmos14010178

Chen J, Zhou M, Yang J, Yin P, Wang B, Ou CQ, Liu Q (2020) The modifying effects of heat and cold wave characteristics on cardiovascular mortality in 31 major Chinese cities. Environ Res Lett 15(10):105009. https://doi.org/10.1088/1748-9326/abaea0

Chen H, He W, Sun J, Chen L (2022) Increases of extreme heat-humidity days endanger future populations living in China. Environ Res Lett 17(6):064013. https://doi.org/10.1088/1748-9326/ac69fc

Cheng L, Gu K, Zhao L, Wang H, Ji JS, Liu Z, Huang C (2023) Projecting future labor losses due to heat stress in China under climate change scenarios. Sci Bull 68(22):2827–2837. https://doi.org/10.1016/j.scib.2023.09.044

Eman K, Chung ES, Ayugi BO (2024) Investigating the skills of highresmip in capturing historical and future mean precipitation shifts over Pakistan. Int J Climatol 44(11):3888–3911. https://doi.org/10.1002/joc.8558

Esfahani MT, Awolusi I, Hatipkarasulu Y (2024) Effects of heat stress prevention training on the knowledge of construction students. Journal Engineering Project Prod Manage 14(2). https://doi.org/10.32738/jeppm-2024-0018

Fanger PO (1970) Thermal comfort: analysis and applications in environmental engineering. Danish Technical, New York, McGraw-Hill, Copenhgen

Foster J, Smallcombe JW, Hodder S, Jay O, Flouris AD, Nybo L, Havenith G (2021) An advanced empirical model for quantifying the impact of heat and climate change on human physical work capacity. Int J Biometeorol 65:1215–1229. https://doi.org/10.1007/s00484-021-02105-0

Gu X, Zhang J (2025) Green and grey cooling: mitigating pedestrians perceived temperature via urban shades. Build Environ 113585. https://doi.org/10.1016/j.buildenv.2025.113585

Havenith G, Fiala D (2011) Thermal indices and thermophysiological modeling for heat stress. Compr Physiol 6(1):255–302. https://doi.org/10.1002/cphy.c140051

He W, Chen H (2023) More extreme-heat occurrences related to humidity in China. Atmos Ocean Sci Lett 16(5):100391. https://doi.org/10.1016/j.aosl.2023.100391

He W, Chen H, Ma J (2023) Variations in summer extreme hot–humid events over Eastern China and the possible associated mechanisms. J Clim 36(11):3801–3815. https://doi.org/10.1175/JCLI-D-22-0695.1

Hersbach H, Bell B, Berrisford P, Biavati G, Horányi A, Muñoz Sabater J, Nicolas J, Peubey C, Radu R, Rozum I, Schepers D, Simmons J-N (2023) ERA5 hourly data on single levels from 1940 to present [dataset]. Copernicus Climate Change Service (C3S) Climate Data Store (CDS). https://doi.org/10.24381/cds.adbb2d47

Huang L, He Y, Ruan W (2024) Evaluation and projection of extreme climate indices in Southwest China by CMIP6 models. Journal of Yunnan University: Natural Sciences Edition 46(4):686–696

Johansson E, Emmanuel R (2006) The influence of urban design on outdoor thermal comfort in the hot, humid City of Colombo, Sri Lanka. Int J Biometeorol 51:119–133. https://doi.org/10.1007/s00484-006-0047-6

Karlsson K-G, Riihelä A, Trentmann Jörg et al (2023) CLARA-A3: CM SAF cLoud, Albedo and surface RAdiation dataset from

AVHRR data - Edition 3 [dataset]. Satellite Application Facility on Climate Monitoring. https://doi.org/10.5676/EUM_SAF_CM/CLARA_AVHRR/V003

Kjellstrom T, Holmer I, Lemke B (2009a) Workplace heat stress, health and productivity–an increasing challenge for low and middle-income countries during climate change. Glob Health Action 2(1):2047. https://doi.org/10.3402/gha.v2i0.2047

Kjellstrom T, Kovats RS, Lloyd SJ, Holt T, Tol RS (2009b) The direct impact of climate change on regional labor productivity. Arch Environ Occup Health 64(4):217–227. https://doi.org/10.1080/19338240903352776

Kjellstrom T, Freyberg C, Lemke B, Otto M, Briggs D (2018) Estimating population heat exposure and impacts on working people in conjunction with climate change. Int J Biometeorol 62(3):291–306. https://doi.org/10.1007/s00484-017-1407-0

Kong Q, Huber M (2022) Explicit calculations of wet-bulb globe temperature compared with approximations and why it matters for labor productivity. Earths Future 10(3):e2021EF002334. https://doi.org/10.1029/2021EF002334

Lemke B, Kjellstrom T (2012) Calculating workplace WBGT from meteorological data: a tool for climate change assessment. Ind Health 50(4):267–278. https://doi.org/10.2486/indhealth.MS1352

Li X, Chow KH, Zhu Y, Lin Y (2016) Evaluating the impacts of high-temperature outdoor working environments on construction labor productivity in China: a case study of rebar workers. Build Environ 95:42–52. https://doi.org/10.1016/j.buildenv.2015.09.005

Li D, Yuan J, Kopp RE (2020) Escalating global exposure to compound heat-humidity extremes with warming. Environ Res Lett 15(6):064003. https://doi.org/10.1088/1748-9326/ab7d04

Li L, Li J, Yu R (2022) Evaluation of CMIP6 highresmip models in simulating precipitation over central Asia. Adv Clim Change Res 13(1):1–13. https://doi.org/10.1016/j.accre.2021.09.009

Liljegren JC, Carhart RA, Lawday P, Tschopp S, Sharp R (2008) Modeling the wet bulb Globe temperature using standard meteorological measurements. J Occup Environ Hyg 5(10):645–655. https://doi.org/10.1080/15459620802310770

Liu YC, Fan J, Zhang GJ, Xu KM, Ghan SJ (2015) Improving representation of convective transport for scale-aware parameterization: 2. Analysis of cloud-resolving model simulations. J Geophys Res Atmos 120(8):3510–3532. https://doi.org/10.1002/2014JD022142

Liu Y, Zhang Z, Chen X, Huang C, Han F, Li N (2021) Assessment of the regional and sectoral economic impacts of heat-related changes in labor productivity under climate change in China. Earths Future 9(8):e2021EF002028. https://doi.org/10.1029/2021EF002028

Middel A, AlKhaled S, Schneider FA, Hagen B, Coseo P (2021) 50 grades of shade. Bull Am Meteorol Soc 102(9):E1805–E1820. https://doi.org/10.1175/BAMS-D-20-0193.1

Panda KC, Singh RM, Thakural LN, Sahoo DP (2022) Representative grid location-multivariate adaptive regression spline (RGL-MARS) algorithm for downscaling dry and wet season rainfall. J Hydrol 605:127381. https://doi.org/10.1016/j.jhydrol.2021.127381

Parsons LA, Shindell D, Tigchelaar M, Zhang Y, Spector JT (2021) Increased labor losses and decreased adaptation potential in a warmer world. Nat Commun 12(1):7286. https://doi.org/10.1038/s41467-021-27328-y

Parsons LA, Masuda YJ, Kroeger T, Shindell D, Wolff NH, Spector JT (2022) Global labor loss due to humid heat exposure underestimated for outdoor workers. Environ Res Lett 17(1):014050. https://doi.org/10.1088/1748-9326/ac3dae

Qiao Y, Qiao L, Chen Z, Liu B, Gao L, Zhang L (2022) Wearable sensor for continuous sweat biomarker monitoring. Chemosensors 10(7):273. https://doi.org/10.3390/chemosensors10070273

Roberts M (2019a) MOHC HadGEM3-GC31-HH model output prepared for CMIP6 highresmip highres-future. Earth Syst Grid Federation. https://doi.org/10.22033/ESGF/CMIP6.5982

Roberts M (2019b) MOHC HadGEM3-GC31-HM model output prepared for CMIP6 highresmip highres-future. Earth Syst Grid Federation. https://doi.org/10.22033/ESGF/CMIP6.5984

Roberts MJ, Baker A, Blockley EW, Calvert D, Coward A, Hewitt HT, Vidale PL (2019) Description of the resolution hierarchy of the global coupled HadGEM3-GC3. 1 model as used in CMIP6 HighResMIP experiments. Geosci Model Dev 12(12):4999–5028. https://doi.org/10.5194/gmd-12-4999-2019

Rowlinson S, YunyanJia A, Li B, ChuanjingJu C (2014) Management of climatic heat stress risk in construction: a review of practices, methodologies, and future research. Accid Anal Prev 66:187–198. https://doi.org/10.1016/j.aap.2013.08.011

Runkle JD, Cui C, Fuhrmann C, Stevens S, Del Pinal J, Sugg MM (2019) Evaluation of wearable sensors for physiologic monitoring of individually experienced temperatures in outdoor workers in southeastern US. Environ Int 129:229–238. https://doi.org/10.1016/j.envint.2019.05.026

Sahu S, Sett M, Kjellstrom T (2013) Heat exposure, cardiovascular stress and work productivity in rice harvesters in India: implications for a climate change future. Ind Health 51(4):424–431. https://doi.org/10.2486/indhealth.2013-0006

Shakerian S, Habibnezhad M, Ojha A, Lee G, Liu Y, Jebelli H, Lee S (2021) Assessing occupational risk of heat stress at construction: a worker-centric wearable sensor-based approach. Saf Sci 142:105395. https://doi.org/10.1016/j.ssci.2021.105395

Sheng R, Li C, Wang Q, Yang L, Bao J, Wang K, Huang C (2018) Does hot weather affect work-related injury? A case-crossover study in Guangzhou, China. Int J Hyg Environ Health 221(3):423–428. https://doi.org/10.1016/j.ijheh.2018.01.005

Song S, Zhang F (2022) A study on assessing the awareness of heat-related illnesses in the construction industry. In Construction Research Congress 2022 (pp. 431–440). https://doi.org/10.1061/9780784483985.044

Sun Y, Hu T (2023) Detection of the anthropogenic signal and urbanization effects in extreme temperature changes in eastern China. Atmos Ocean Sci Lett 16(2):100332. https://doi.org/10.1016/j.aosl.2023.100332

Sun S, Li L, Yang ZL, Wang G, McDowell NG, Matheny AM, Wang D (2024) Refining water and carbon fluxes modeling in terrestrial ecosystems via plant hydraulics integration. Agric For Meteorol 359:110256. https://doi.org/10.1016/j.agrformet.2024.110256

Sun Y, Zhu S, Wang D, Duan J, Lu H, Yin H, Guan D (2024b) Global supply chains amplify economic costs of future extreme heat risk. Nature 627(8005):797–804. https://doi.org/10.1038/s41586-024-07147-z

Terai CR, Caldwell PM, Klein SA, Tang Q, Branstetter ML (2018) The atmospheric hydrologic cycle in the ACME v0. 3 model. Clim Dyn 50(9):3251–3279. https://doi.org/10.1007/s00382-017-3803-x

Torbat Esfahani M, Awolusi I, Hatipkarasulu Y (2024) Heat stress prevention in construction: a systematic review and meta-analysis of risk factors and control strategies. Int J Environ Res Public Health 21(12):1681. https://doi.org/10.3390/ijerph21121681

Wang P, Yang Y, Tang J, Leung LR, Liao H (2021) Intensified humid heat events under global warming. Geophys Res Lett 48(2):e2020GL091462. https://doi.org/10.1029/2020GL091462

Wang R, Wang Z, Gao R, Ye D (2023) Climatology and changing trend of the regional high temperature process in China during 1961–2020. Chinese Journal of Geophysics (in Chinese), 66(2), 494–504.s. https://doi.org/10.6038/cjg2022P0756

Wang L, Zhu J, Wang D (2025) Comparative analysis of high-resolution CMIP6 GCM and CMIP5 RCM: unveiling biases and advancements in simulating compound extreme events in China.

Clim Dyn 63(1):1–22. https://doi.org/10.1007/s00382-024-07571-x

Wei J, Ting D, Hui G, Zhuozhuo L (2024) China's Yangtze river basin is becoming the super heatwave centre in the East Asian monsoon regions. Int J Climatol 44(14):5028–5038. https://doi.org/10.1002/joc.8621

Wu J, Gao X (2013) A gridded daily observation dataset over China region and comparison with the other datasets [dataset]. Chin J Geophys 56(4):1102–1111. https://doi.org/10.6038/cjg20130406

Wyndham CH (1969) Adaptation to heat and cold. Environ Res 2(5–6):442–469

Xia Y, Li Y, Guan D, Tinoco DM, Xia J, Yan Z, Huo H (2018) Assessment of the economic impacts of heat waves: a case study of Nanjing, China. J Clean Prod 171:811–819. https://doi.org/10.1016/j.jclepro.2017.10.069

Xu X, Yan J, Liu G, Zhong X (2017) Temporal and Spatial variations of extremely high temperature in China under different emission scenarios of CMIP5. J Cent China Normal Univ (in Chinese), 51(4)

Zhang Z (2011) The relationships between labor productivity and value of commodities: the micro-rules and macro-characteristics. China Rev Polit Econ 2(2):72–92

Zhang Z, Zhang GJ (2022) Dependence of convective cloud properties and their transport on cloud fraction and GCM resolution diagnosed from a cloud-resolving model simulation. J Mar Sci Eng 10(9):1318. https://doi.org/10.3390/jmse10091318

Zhang Y, Sun Y, Hu T (2024) Changes in extreme high temperature warning indicators over China under different global warming levels. Sci China Earth Sci 67(6):1895–1909. https://doi.org/10.1007/s11430-023-1299-1

Zhao M, Lee JKW, Kjellstrom T, Cai W (2021) Assessment of the economic impact of heat-related labor productivity loss: a systematic review. Clim Change 167(1):22. https://doi.org/10.1007/s10584-021-03160-7

Zheng D, Huang X, Pan A (2023) Evaluation of high temperature on urban economic losses from the perspective of labor productivity. Econ Geogr 43(6):13–21. https://doi.org/10.15957/j.cnki.jjdl.2023.06.002